

Article

Plasma Sputtered Tungsten Oxide Thin Film on Poly(lactic acid) for Food Packaging Applications

Matteo Pedroni ^{1,*}, Espedito Vassallo ¹, Marco Aloisio ¹, Milena Brasca ², Hao Chen ^{3,4}, Giuseppe Firpo ⁵, Francesco Ghezzi ¹, Stefano Morandi ², Silvia Maria Pietralunga ^{4,6}, Tiziana Silveti ² and Tersilla Virgili ⁶

¹ Institute for Plasma Science and Technology (ISTP), National Research Council-CNR, Via R. Cozzi 53, 20125 Milan, Italy; espedito.vassallo@istp.cnr.it (E.V.); marco.aloisio@istp.cnr.it (M.A.); francesco.ghezzi@istp.cnr.it (F.G.)

² Institute of Sciences of Food Production (ISPA), National Research Council-CNR, Via G. Celoria 2, 20133 Milan, Italy; milena.brasca@ispa.cnr.it (M.B.); stefano.morandi@ispa.cnr.it (S.M.); tiziana.silveti@ispa.cnr.it (T.S.)

³ Department of Physics, Politecnico di Milano, Piazza Leonardo da Vinci 32, 20133 Milan, Italy; hao.chen@polimi.it

⁴ Istituto Italiano di Tecnologia (IIT), Center for Nano Science and Technology, Via Pascoli 10, 20133 Milan, Italy; silvia.pietralunga@polimi.it

⁵ Department of Physics, University of Genoa, Via Dodecaneso 33, 16145 Genova, Italy; firpo@fisica.unige.it

⁶ National Research Council-CNR, Institute for Photonics and Nanotechnologies (IFN), Piazza Leonardo da Vinci 32, 20133 Milan, Italy; tersilla.virgili@polimi.it

* Correspondence: matteo.pedroni@istp.cnr.it; Tel.: +39-02-66173215



Citation: Pedroni, M.; Vassallo, E.; Aloisio, M.; Brasca, M.; Chen, H.; Firpo, G.; Ghezzi, F.; Morandi, S.; Pietralunga, S.M.; Silveti, T.; et al. Plasma Sputtered Tungsten Oxide Thin Film on Poly(lactic acid) for Food Packaging Applications. *Coatings* **2021**, *11*, 1281. <https://doi.org/10.3390/coatings11111281>

Academic Editor: Andrzej Lenart

Received: 27 September 2021

Accepted: 19 October 2021

Published: 21 October 2021

Publisher's Note: MDPI stays neutral with regard to jurisdictional claims in published maps and institutional affiliations.



Copyright: © 2021 by the authors. Licensee MDPI, Basel, Switzerland. This article is an open access article distributed under the terms and conditions of the Creative Commons Attribution (CC BY) license (<https://creativecommons.org/licenses/by/4.0/>).

Abstract: Biodegradable and bio-derived plastics such as poly(lactic acid) (PLA) are a promising solution to solve the huge environmental and economic issues caused by the enormous consumption of conventional oil-derived polymers, especially in food packaging applications. However, their poor gas barrier properties and high transparency to UV radiation limit their currently commercialization. Therefore, this study is focused on the deposition of tungsten oxide (WO_x) thin films on commercial PLA in order to enhance its overall performance. Coatings with different thickness (25, 50 and 100 nm) were deposited by means of radiofrequency (RF) plasma magnetron reactive sputtering. Morphological characterization was carried out with atomic force microscopy (AFM) and scanning electron microscopy (SEM). In order to evaluate surface chemical changes due to plasma treatments, Fourier-transform infrared spectroscopy (FTIR) and X-ray photoelectron spectroscopy (XPS) analysis were performed. The PLA/WO_x samples demonstrated remarkable improvements both in UV protection and oxygen barrier properties. In particular, light transmittance was reduced by approximately 95% in the UV-B region, 70% in the UV-A region and 50% in the visible region compared to pristine PLA. Regarding oxygen permeation, a reduction of at least 99.9% was achieved. In addition, the PLA/WO_x antibacterial properties against *Escherichia coli* were also investigated, showing a reduction greater than 5 log₁₀ CFU cm⁻² after 24 h for the 50 and 100 nm samples. These results demonstrate the potential of WO_x thin coating for sustainable food packaging applications.

Keywords: reactive sputtering; tungsten oxide; poly(lactic acid); biodegradable; food packaging; oxygen barrier; UV protection; antimicrobial properties

1. Introduction

Biodegradable polymers and green packaging are viewed as a feasible strategy to reduce the serious environmental problem caused by the excessive use of conventional plastic polymers as packaging materials [1]. Among the possible biopolymer candidates, poly(lactic acid) (PLA) [2,3] is one with the highest commercial potential due to its biocompatibility, transparency and mechanical properties comparable with those of conventional polymers [4,5]. However, its permeable nature to gas along with its transparency to UV radiation restrict its use for several applications, especially related to food packaging [6,7].

Overcoming these drawbacks is fundamental to estimate and extend the food shelf life. In fact, both oxygen and UV light lead to oxidation processes which alter food quality and produce toxic compounds [8,9]. Moreover, PLA backbone readily undergoes degradation and weakening when exposed to artificial and sun light UV radiation. This results in a color change of the polymer and further UV light transmittance [7]. Therefore, it becomes primarily important to enhance the barrier and the UV protective properties of PLA.

In this view, metal oxides UV absorber have attracted significant interest in recent years [10,11]. Titanium dioxide (TiO₂) [12,13], magnesium oxide (MgO) [14], cerium oxide (CeO₂) [15] and zinc oxide (ZnO) [8,16] are the most commonly studied by the scientific community. However, no studies on tungsten oxide (WO_x) are reported in literature despite its strong photoabsorption properties [17–19] and a safety assessment for use in food contact materials released by EFSA [20]. Safety evaluations were conducted for polyethylene terephthalate (PET) where WO_x was used as a reheat agent. It is specified that for other technical functions or for use in different polymers, further migration tests should be performed.

Finally, WO_x can also be used as an antibacterial agent [21], obtaining an active food packaging which can prevent foodborne diseases [22]. Thus, the aim of this study is to investigate the effect of WO_x thin films deposited on PLA concerning the oxygen permeation, UV transmittance and antibacterial activity against *Escherichia coli*. WO_x coatings were obtained by RF magnetron plasma sputtering which ensures the deposition of high-quality oxide barrier layers and low process temperatures in order to not damage polymer substrates [21,22].

2. Materials and Methods

2.1. Coatings Preparation

WO_x thin coatings (25, 50, 100 nm) were deposited on PLA (Coralene SW PLA, Corapack) by means of RF (13.56 MHz) plasma magnetron sputtering using 3-inch W metal target (Testbourne Ltd., Hampshire, UK, purity of 99.99%) in a reactive environment (Ar/O₂). As suggested by Fahlteich et al. [23], we worked in transition mode, i.e., the highest deposition rate that allows transparent coatings. In our case, this corresponded to 30% O₂ in the gas mixture. The power was set at 75 W, the working pressure was 2 Pa and the polymers were placed on the substrate holder at 6.5 cm from the target. In order to determine the deposition rate (nm/min) and thus predict the thickness of the coatings, preliminary depositions on silicon (<100>, 380 ± 25 μm, Si-Mat Silicon Materials, Kaufering, Germany) were performed. A portion of the sample was covered with a silicon mask during the process. Upon removing it, it was possible to measure the height difference between deposited and non-deposited portions of the sample with a P15 surface profiler (KLA Tencor, San Jose, CA, USA). The calculated deposition rate was 50 nm/min. The substrate temperature during the processes never exceeded 55 °C. Prior to each deposition, the target was sputter cleaned by means of an Ar Plasma for 15 min at 1 Pa. This procedure is necessary to prevent target poisoning and consequent non-reproducible depositions [24].

2.2. Samples Characterization

The surface morphology of the samples was characterized by Atomic Force Microscopy (AFM) (Core AFM, Nanosurf GmbH, Langen, Germany) in dynamic mode and scanning electron microscope (SEM) (Tescan mod. MIRA III, Brno, Czech Republic). The AFM images were post-processed with Gwyddion software. For accurate SEM imaging samples were metallized by depositing an ultra-thin layer of gold by sputtering (about 8 nm) to provide discharging, and high-resolution images were taken at 5 kV of electron beam voltage, while optimizing beam current and pixel dwell time. Chemical structure was investigated by Fourier-transform infrared spectroscopy (FTIR) (Spectrum Two, PerkinElmer, Milan, Italy) and X-ray photoelectron spectroscopy (XPS) was used for surface chemical characterization. The XPS apparatus consisted of a VSW CLASS 100 hemispherical analyzer, equipped with a single channel detector, with a non-monochromatic Al/Mg X-ray source (VSW model

TA10). The apparatus was equipped with an impact ionization ion gun VG EX05 with a raster scan unit (SAX 346) for imaging and depth profiling. Ar, Ne and He gas could be used. Core level spectra were acquired using a non-monochromatized Al anode X-ray source ($h\nu = 1486.6$ eV) VSW model TA10 and a hemispherical analyzer VSW model CLASS 100, equipped with a single channel detector, operating in constant Pass Energy mode (44 eV) with 0.9 eV of overall resolution. Wide scan spectra were acquired with 2 eV of resolution. All spectra were referenced to the same energy scale determined by calibrating the Ag 3d5/2 line at 368.3 eV. The Atomic Sensitivity Factors were determined as reported in detail in [25]. The sample surfaces were first cleaned by a gentle sputtering with Ar at 4.5 keV for 60 min at a current density of 15 nA/cm² stepwise of 30 in order to remove the adventitious carbon. Optical properties were studied using a Spectrophotometer UV-VIS-NIR (V-570, Jasco, Cremella (LC), Italy).

Permeability to O₂ was measured with a high vacuum experimental set up reported in reference [26]. The apparatus measures gas permeability in manometric procedures by means of a mass spectrometer. Its results are accurate in a range spanning several orders of magnitude, including permeability values of packaging materials. Another benefit is to provide traceability of measurements by in situ calibration without losing the advantages of a state-of-the-art commercial apparatus; rather, thanks to the mass spectrometer, it is possible to measure the gas transmission rate directly, rapidly and selectively with any tracer gas.

The antimicrobial activity was evaluated against *Escherichia coli* ATCC 8739 from the American Type Culture Collection (ATCC, Manassas, VA, USA). The strain was maintained in Brain Heart Infusion (BHI) broth (Biolife Italiana, Milan, Italy) and cultured in BHI under aerobic conditions at 37 °C overnight prior to use in experiment. A standard colony-forming units (CFU) assay was performed to determine the reduction in bacterial viability after 24 h of incubation in contact with the material. For this purpose, both the pristine PLA and the different (25, 50 and 100 nm) WO_x-coated PLA films were cut in a disk shape of 2 cm diameter, placed into a sterile 12-well microplate with a lid (Cellstar, Greiner Bio-One, Frickenhausen, Germany) and sterilized under a UV ray for 30 min. In the microplate, each material (pristine PLA, 25 nm WO_x/PLA, 50 nm WO_x/PLA and 100 nm WO_x/PLA) was present in duplicate. The remaining wells of the microplate were filled with sterile distilled water to maintain a humid environment within the microplate during the 24 h incubation and to prevent drying of the inocula. *Escherichia coli* inocula were obtained by diluting the strain culture (dilution = 1:1000, corresponding to about 10⁶ CFU mL⁻¹) in quarter-strength Ringer's solution (Scharlau Microbiology, Barcelona, Spain). The concentration of the bacterial suspension was quantified using Petrifilm Aerobic Count plate (3M Minneapolis, MN, USA) with incubation at 37 °C for 24 h. Then, 100 µL aliquots of the strain suspension were used to inoculate each disc in the microplate. The microplate was incubated for 24 h at room temperature under static conditions. After incubation, the bacterial suspension on each disc was taken with a micropipette and transferred in a sterile Stomacher bag. Each disc was then removed with sterile tweezers and placed in the Stomacher bag, added with Ringer's solution to give 1:100 dilution and homogenized for 2 min. Thereafter, ten-fold serial dilutions were used to enumerate the bacterial strain on Petrifilm Aerobic Count plate. The plates were incubated at 37 °C for 24 h, the number of CFU determined and the results expressed as log₁₀ CFU cm⁻² (mean values ± standard error).

3. Results and Discussions

3.1. Morphological Analysis

Figure 1 shows the AFM images of the pristine PLA and the PLA coated with different WO_x thickness. The coatings have a ripple-like morphology caused by thermally induced residual stress [27–29]. The accumulated thermal stress arises both from gas atoms impinging the growing film and the marked difference between the thermal expansion coefficient of WO_x and PLA. Therefore, the deposition process at a temperature close to the glass transition temperature of PLA, i.e., 57 °C [30] induced significant morphological

changes compared to flat pristine PLA. These nanostructures cause an increase in the surface average roughness, which rises from 6 nm for the pristine PLA to 24, 59 and 140 nm for the 25, 50 and 100 nm PLA/WO_x, respectively. The SEM images of the 25 nm PLA/WO_x (Figure 2) confirm the coating growth morphology.

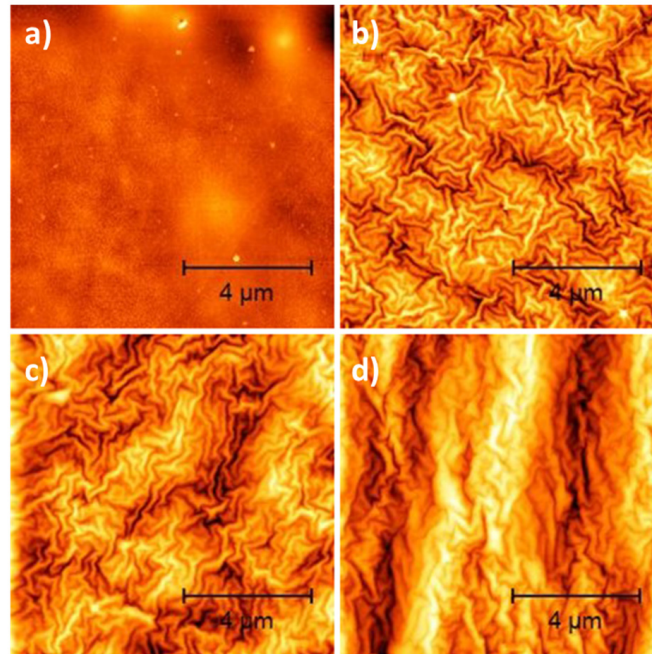


Figure 1. AFM images of (a) pristine PLA and (b) PLA/25 nm WO_x, (c) PLA/50 nm WO_x and (d) PLA/100 nm WO_x.

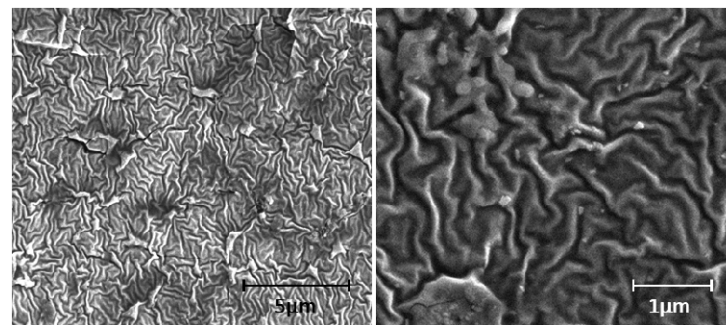


Figure 2. SEM image of PLA/25 nm WO_x at different magnifications.

3.2. Chemical Structure Analysis

Figure 3 shows the FTIR spectrum for pristine PLA and the WO_x-coated PLA, respectively. No evident differences between the peak positions of PLA and the WO_x series are observable. Thus, it is possible to affirm that the plasma deposition process does not significantly affect the chemical structure of the polymer, at least for low thickness coatings. A qualitative analysis bands ratio (Figure 4) supports this last statement. The ratios of C-H (2997 cm⁻¹)/C=O (1747 cm⁻¹) and C-O (1180 cm⁻¹)/C=O (1747 cm⁻¹) remain essentially unchanged for coating thicknesses up to 50 nm. These results qualitatively indicate that no change in the chemical structure of PLA was found in that range of thickness. The decrease in the C-H/C=O ratio indicates an oxidation of the surface during the film depositions [31], and the presence of a new peak at 950 cm⁻¹ in the spectra is attributable to the stretching vibration of W=O [32].

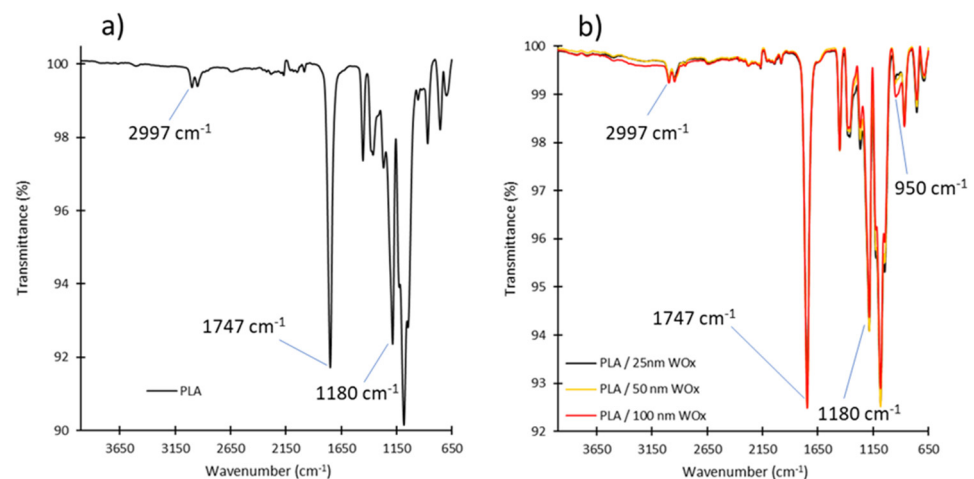


Figure 3. FTIR spectra of (a) pristine PLA and (b) PLA/WO_x samples.

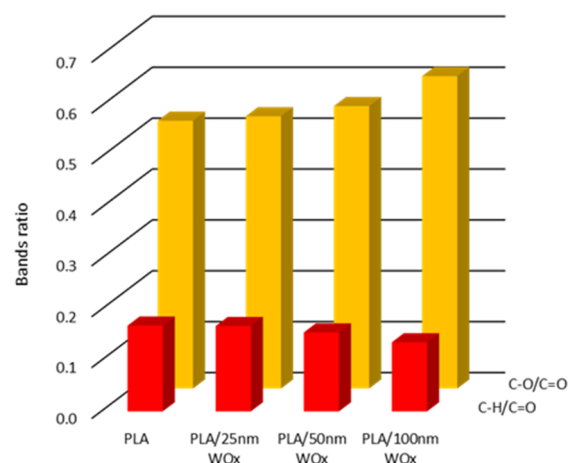


Figure 4. C-H/C=O and C-O/C=O band ratios for pristine PLA and PLA WO_x.

Si coated with 100 nm of WO_x was examined by XPS in order to evaluate the film stoichiometry. The survey scan revealed the presence at the surface of O, C, W and N only and, therefore, is not reported for brevity. Figure 5 reports the high-resolution spectra for the C1s, N1s and W4f levels, respectively. The details of the fitting procedure are reported in reference [25]. The N1s core level was not fitted because the intensity was too low. However, the relative concentrations are reported in Table 1 for all four elements. The O/W ratio was 2.29, thus indicating a sub-stoichiometric composition of the coatings. As reported from [17,33], oxygen-deficient WO_x are of particular interest in various applications due to their strong photoabsorption properties.

The fitting of the C1s level revealed the presence of five contributions. The peak at binding energy (BE) 283.5 eV is assigned to a WC specie, that at BE 284.6 eV to the C-C graphitic bond and those at BE 287.7 and 289 to unspecified hydrocarbons. The presence of WC could be explained by the reactivity of tungsten oxide film for the adsorption of hydrocarbons still present as traces in the residual gas phase of the preparation chamber [34]. The fitting of the W4f line revealed the presence of four components. The peak at BE 32.2 eV is assigned to the WC, in agreement with the results of the C1s level, that at Be 33.6 eV to WO₂, that at BE 34.9 eV to a non-stoichiometric tungsten oxide and that at Be 36.2 eV to the WO₃ specie [35]. As a further cross check, the fitting of the O1s level gave three components. That at BE 530.4 eV is assigned at the WO₂ specie, that at Be 531.4 eV to the non-stoichiometric tungsten oxide and that at 532.7 eV to the WO₃ specie.

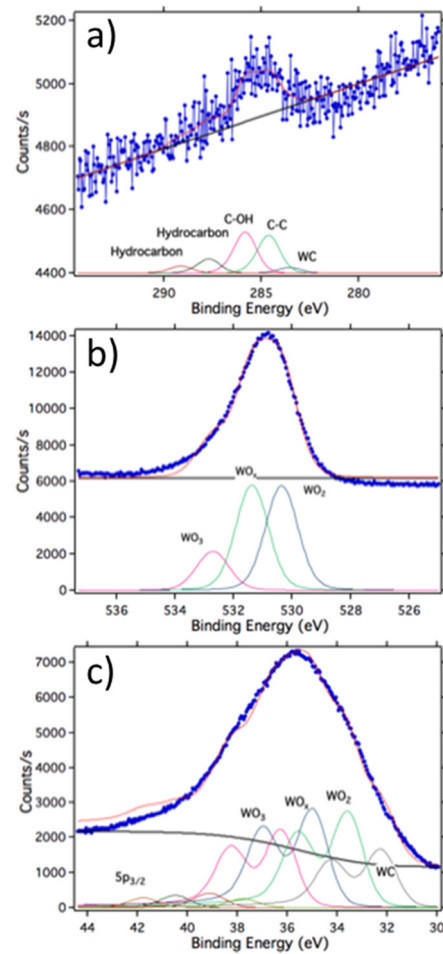


Figure 5. High-resolution spectra; (a) C1s core level, (b) O1s core level and (c) W4f core level.

Table 1. Relative concentrations of the elements revealed at the WO_x surface.

Element	Relative Concentration (%)
N	7.29
O	60.83
C	5.3
W	26.59

3.3. Optical Analysis

The photos reported in Figure 6 show how the transparency of the pristine PLA and the coated ones is similar, regardless of the WO_x thickness. This is fundamental in applications when foods within the packaging must be visible to customers.



Figure 6. Photos of pristine PLA and PLA coated with three different WO_x coating thicknesses.

From Figure 7, it can be seen how the transmittance of the PLA/ WO_x samples decreases significantly over the UV-visible wavelength range compared to the pristine PLA. This confirms the suitable photoabsorption properties of sub-stoichiometric tungsten oxides. The detailed percentage values of transmittance in the UV and visible range are

reported in Table 2. It turns out that pristine PLA can be considered as fully transparent. In fact, its transmittance is about 90% both in the UV and visible regions (from 250 nm to 600 nm). Similar findings have been reported in the literature [7]. Light absorption from WO_x increases with increasing thickness up to 50 nm. Larger film thicknesses do not result in further significant light absorption within the thickness range considered. In particular, the 50 and 100 nm WO_x samples reduce light transmittance by about 95% in the UV-B region (300 nm), 70% in the UV-A region (350 nm) and 50% in the visible region (600 nm) compared to pristine PLA. Interestingly, besides significantly reducing the passage of UV radiation, WO_x coatings also limit the transmittance in the visible region preserving the polymer transparency (Figure 6). This can be fundamental to preserve food quality. In fact, visible light wavelengths may also cause considerable deteriorations to some nutrients, bioactive compounds and pigments [36].

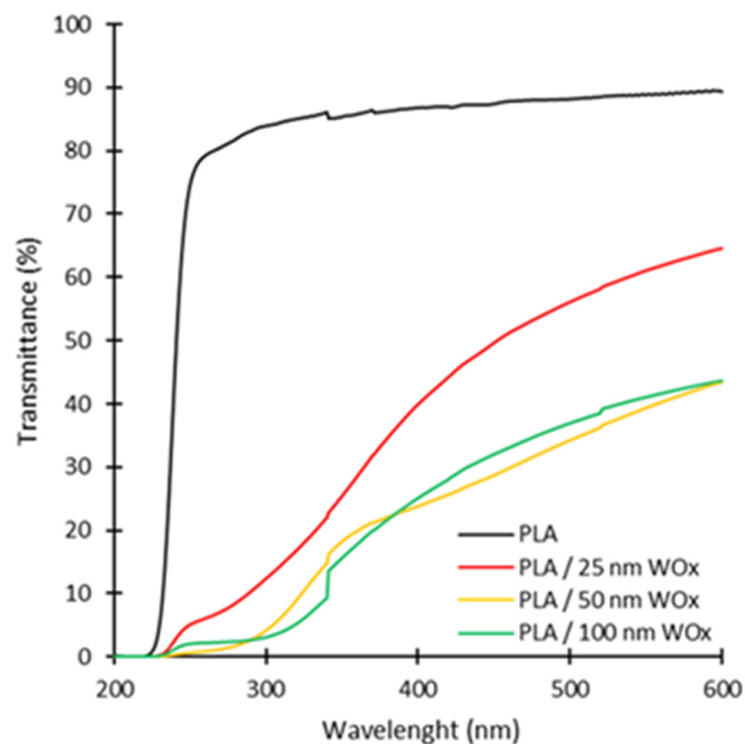


Figure 7. UV-vis absorption spectra of PLA and PLA/WO_x.

Table 2. Percentage of light transmittance (%) in UV and visible regions for PLA and PLA/WO_x.

Sample	Transmittance (%)		
	At 300 nm (UV-B Region)	At 350 nm (UV-A Region)	At 600 nm (Visible Region)
PLA	84	85	89
PLA/25 nm WO _x	12	25	65
PLA/50 nm WO _x	4	18	43
PLA/100 nm WO _x	3	15	44

3.4. Oxygen Permeability Analysis

Oxygen Permeability (OP) data for the pristine and coated PLA films are reported in Figure 8. Uncoated PLA exhibits a permeability of $290 \times 10^{-16} \text{ cm}^3 \cdot \text{cm} / \text{cm}^2 \cdot \text{s} \cdot \text{Pa}$. This result is in accordance with Zhang et al. [34]. The addition of WO_x coatings leads to a substantial enhancement of the polymer barrier properties. In particular, the lowest oxygen permeability was obtained for the 25 nm WO_x sample while higher values were

found for the thicker samples, i.e., 50 and 100 nm. This can be ascribed to intrinsic coating stress which increase with increasing thickness and introduce layer defects [37,38] through which gas transport takes place [23]. The lower permeability value of the 100 nm sample compared to the 50 nm one is probably due to greater film thickness, which increases the path of the permeating gas and partially compensates for the layer defects formation. In any case, an OP reduction of at least 99.9% compared to the pristine PLA was reached for the WO_x samples. According to literature [39], all the coated samples can therefore be classified as having a high oxygen barrier, i.e., $OP < 0.46 \times 10^{-16} \text{ cm}^3 \cdot \text{cm} / \text{cm}^2 \cdot \text{s} \cdot \text{Pa}$.

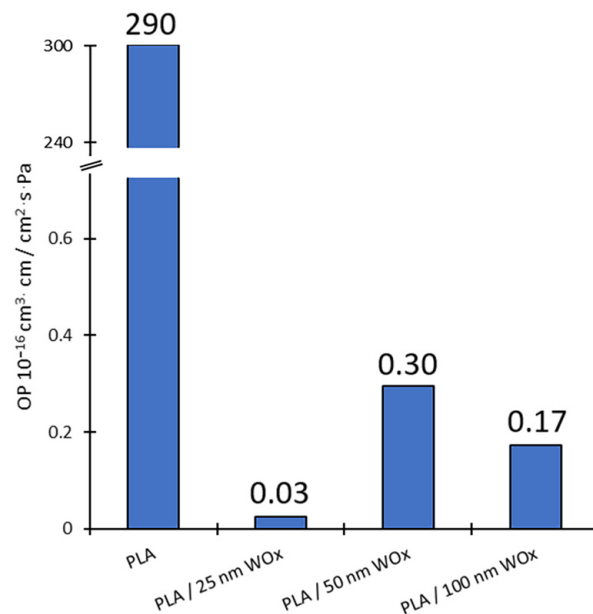


Figure 8. Permeability values to oxygen for PLA and the PLA/WO_x samples.

3.5. Antimicrobial Analysis

The enumeration of the initial bacterial suspension confirmed that it contained $6.20 \pm 0.02 \log_{10} \text{ CFU mL}^{-1}$. Table 3 shows the *Escherichia coli* reduction after 24 h incubation in contact with the WO_x-coated PLA in comparison with pristine PLA. These preliminary results confirm the excellent antimicrobial activity of WO_x coatings against *Escherichia coli*, as recently reported by Tan et al. [21]. However, there exists a minimum thickness, under which bacterial survival is not negatively affected. In fact, *Escherichia coli* cells in contact with the 50 and 100 nm WO_x/PLA were reduced below the detection limit (logarithmic reduction $> 5 \log_{10} \text{ CFU cm}^{-2}$), while the 25 nm WO_x/PLA induced a logarithmic reduction of ~ 1 log with respect to the control, i.e., PLA, under the tested conditions. This weaker antimicrobial activity of the thinner coating could be due to an insufficient active surface area in relation to the *Escherichia coli* inoculum size. In fact, the average roughness, which is a key factor to enhance the bactericidal activity [40], increases significantly with increasing WO_x thickness, as evidenced from the AFM images analysis.

Table 3. *Escherichia coli* viability expressed as $\log_{10} \text{ CFU cm}^{-2}$ (mean values \pm standard error) after 24 h contact with PLA and WO_x-coated PLA.

Sample	<i>Escherichia coli</i>
PLA	6.71 ± 0.07
PLA/25 nm WO _x	5.68 ± 1.49
PLA/50 nm WO _x	<1.49
PLA/100 nm WO _x	<1.49

4. Conclusions

PLA coated with WO_x thin films showed improved properties such as barrier to oxygen, UV light protection and antimicrobial activity. The sputtering deposition technique ensured the fabrication of high quality and homogeneous sub-stoichiometric tungsten oxide coatings. In terms of applications, the best overall performances were provided by coating thicknesses of 50 and 100 nm. Both are characterized by a light transmittance reduction of about 95% in the UV-B region, 70% in the UV-A region and 50% in the visible region with respect to pristine PLA. Moreover, they showed high oxygen barrier properties, i.e., OP < 0.46 × 10⁻¹⁶ cm³·cm/cm²·s·Pa, and excellent antimicrobial activity against *E. coli* with a reduction greater than 5 log₁₀ CFU cm⁻² after 24 h. Since the two coatings have similar performances, the 50 nm one is preferable from the point of view of process scalability and industrialization due less deposition time and minor induced changes in polymer chemical structure (Figure 4).

Author Contributions: M.P. Conceptualization, Methodology, Writing—original draft, Investigation, Writing—review & editing; E.V. Conceptualization, Supervision, Project administration, Funding acquisition; M.A., M.B., T.S., S.M., G.F., F.G., S.M.P., H.C., T.V. Resources, Investigation. All authors have read and agreed to the published version of the manuscript.

Funding: This research was funded by the sPATIALS3 project, which is financed by the European Regional Development Fund under the ROP of the Lombardy Region ERDF 2014–2020- Axis I “Strengthen technological research, development and innovation”, Action 1.b.1.3 “Support for cooperative R&D activities to develop new sustainable technologies, products and services”, Call Hub.

Institutional Review Board Statement: Not applicable.

Informed Consent Statement: Not applicable.

Data Availability Statement: The data presented in this study are available on request from the corresponding author. The data are not publicly available due to privacy.

Acknowledgments: The authors wish to thank Corapack Srl, (Brenna (CO), Italy) for providing PLA substrates.

Conflicts of Interest: The authors declare no conflict of interest.

References

1. Han, J.W.; Ruiz-Garcia, L.; Qian, J.-P.; Yang, X.-T. Food Packaging: A Comprehensive Review and Future Trends. *Compr. Rev. Food Sci. Food Saf.* **2018**, *17*, 860–877. [[CrossRef](#)]
2. Jamshidian, M.; Tehrani, E.A.; Imran, M.; Jacquot, M.; Desobry, S. Poly-Lactic Acid: Production, Applications, Nanocomposites, and Release Studies. *Compr. Rev. Food Sci. Food Saf.* **2010**, *9*, 552–571. [[CrossRef](#)]
3. Siracusa, V.; Rocculi, P.; Romani, S.; Rosa, M.D. Biodegradable Polymers for Food Packaging: A Review. *Trends Food Sci. Technol.* **2008**, *19*, 634–643. [[CrossRef](#)]
4. Alzate Marin, J.C.; Rivero, S.; Pinotti, A.; Caravelli, A.; Zaritzky, N.E. Microstructural Behaviors of Matrices Based on Polylactic Acid and Polyhydroxyalkanoates. *J. Agric. Food Chem.* **2018**, *66*, 10033–10040. [[CrossRef](#)] [[PubMed](#)]
5. Kakroodi, A.R.; Kazemi, Y.; Ding, W.; Ameli, A.; Park, C.B. Poly(Lactic Acid)-Based in Situ Microfibrillar Composites with Enhanced Crystallization Kinetics, Mechanical Properties, Rheological Behavior, and Foaming Ability. *Biomacromolecules* **2015**, *16*, 3925–3935. [[CrossRef](#)] [[PubMed](#)]
6. Wang, J.; Gardner, D.J.; Stark, N.M.; Bousfield, D.W.; Tajvidi, M.; Cai, Z. Moisture and Oxygen Barrier Properties of Cellulose Nanomaterial-Based Films. *ACS Sustain. Chem. Eng.* **2018**, *6*, 49–70. [[CrossRef](#)]
7. Narayanan, M.; Loganathan, S.; Valapa, R.B.; Thomas, S.; Varghese, T.O. UV Protective Poly(Lactic Acid)/Rosin Films for Sustainable Packaging. *Int. J. Biol. Macromol.* **2017**, *99*, 37–45. [[CrossRef](#)]
8. Shahabi-Ghahfarrokhi, I.; Khodaiyan, F.; Mousavi, M.; Yousefi, H. Preparation of UV-Protective Kefiran/Nano-ZnO Nanocomposites: Physical and Mechanical Properties. *Int. J. Biol. Macromol.* **2015**, *72*, 41–46. [[CrossRef](#)]
9. Llorens, A.; Lloret, E.; Picouet, P.A.; Trbojevič, R.; Fernandez, A. Metallic-Based Micro and Nanocomposites in Food Contact Materials and Active Food Packaging. *Trends Food Sci. Technol.* **2012**, *24*, 19–29. [[CrossRef](#)]
10. Garcia, C.V.; Shin, G.H.; Kim, J.T. Metal Oxide-Based Nanocomposites in Food Packaging: Applications, Migration, and Regulations. *Trends Food Sci. Technol.* **2018**, *82*, 21–31. [[CrossRef](#)]
11. Galstyan, V.; Bhandari, M.P.; Sberveglieri, V.; Sberveglieri, G.; Comini, E. Metal Oxide Nanostructures in Food Applications: Quality Control and Packaging. *Chemosensors* **2018**, *6*, 16. [[CrossRef](#)]

12. Krehula, L.K.; Papić, A.; Krehula, S.; Gilja, V.; Foglar, L.; Hrnjak-Murčić, Z. Properties of UV Protective Films of Poly (Vinyl-Chloride)/TiO₂ Nanocomposites for Food Packaging. *Polym. Bull.* **2017**, *74*, 1387–1404. [[CrossRef](#)]
13. Goudarzi, V.; Shahabi-Ghahfarrokhi, I.; Babaei-Ghazvini, A. Preparation of Ecofriendly UV-Protective Food Packaging Material by Starch/TiO₂ Bio-Nanocomposite: Characterization. *Int. J. Biol. Macromol.* **2017**, *95*, 306–313. [[CrossRef](#)] [[PubMed](#)]
14. Swaroop, C.; Shukla, M. Nano-Magnesium Oxide Reinforced Polylactic Acid Biofilms for Food Packaging Applications. *Int. J. Biol. Macromol.* **2018**, *113*, 729–736. [[CrossRef](#)] [[PubMed](#)]
15. Culica, M.E.; Chibac-Scutaru, A.L.; Melinte, V.; Coseri, S. Cellulose Acetate Incorporating Organically Functionalized CeO₂ NPs: Efficient Materials for UV Filtering Applications. *Materials* **2020**, *13*, 2955. [[CrossRef](#)]
16. Marra, A.; Silvestre, C.; Duraccio, D.; Cimmino, S. Polylactic Acid/Zinc Oxide Biocomposite Films for Food Packaging Application. *Int. J. Biol. Macromol.* **2016**, *88*, 254–262. [[CrossRef](#)]
17. Wu, C.-M.; Naseem, S.; Chou, M.-H.; Wang, J.-H.; Jian, Y.-Q. Recent Advances in Tungsten-Oxide-Based Materials and Their Applications. *Front. Mater.* **2019**, *6*. [[CrossRef](#)]
18. Mardare, C.C.; Hassel, A.W. Review on the Versatility of Tungsten Oxide Coatings. *Phys. Status Solidi A* **2019**, *216*, 1900047. [[CrossRef](#)]
19. Cong, S.; Geng, F.; Zhao, Z. Tungsten Oxide Materials for Optoelectronic Applications. *Adv. Mater.* **2016**, *28*, 10518–10528. [[CrossRef](#)]
20. Silano, V.; Bolognesi, C.; Cravedi, J.-P.; Engel, K.-H.; Fowler, P.; Franz, R.; Grob, K.; Gürtler, R.; Husøy, T.; Kärenlampi, S.; et al. Safety Assessment of the Substance ‘Tungsten Oxide’ for Use in Food Contact Materials. *EFSA J.* **2017**, *15*, e04661. [[CrossRef](#)]
21. Tan, G.-L.; Tang, D.; Dastan, D.; Jafari, A.; Shi, Z.; Chu, Q.-Q.; Silva, J.P.B.; Yin, X.-T. Structures, Morphological Control, and Antibacterial Performance of Tungsten Oxide Thin Films. *Ceram. Int.* **2021**, *47*, 17153–17160. [[CrossRef](#)]
22. Huang, T.; Qian, Y.; Wei, J.; Zhou, C. Polymeric Antimicrobial Food Packaging and Its Applications. *Polymers* **2019**, *11*, 560. [[CrossRef](#)]
23. Fahlteich, J.; Fahland, M.; Schönberger, W.; Schiller, N. Permeation Barrier Properties of Thin Oxide Films on Flexible Polymer Substrates. *Thin Solid Films* **2009**, *517*, 3075–3080. [[CrossRef](#)]
24. Berg, S.; Nyberg, T. Fundamental Understanding and Modeling of Reactive Sputtering Processes. *Thin Solid Films* **2005**, *476*, 215–230. [[CrossRef](#)]
25. Ghezzi, F.; Laguardia, L.; Caniello, R.; Canton, A.; Dal Bello, S.; Rais, B.; Anderle, M. XPS, SIMS and FTIR-ATR Characterization of Boronized Graphite from the Thermonuclear Plasma Device RFX-Mod. *Appl. Surf. Sci.* **2015**, *354*, 408–419. [[CrossRef](#)]
26. Firpo, G.; Setina, J.; Angeli, E.; Repetto, L.; Valbusa, U. High-Vacuum Setup for Permeability and Diffusivity Measurements by Membrane Techniques. *Vacuum* **2021**, *191*, 110368. [[CrossRef](#)]
27. Slepíčka, P.; Fidler, T.; Vasina, A.; Švorčík, V. Ripple-like Structure on PLLA Induced by Gold Deposition and Thermal Treatment. *Mater. Lett.* **2012**, *79*, 4–6. [[CrossRef](#)]
28. Slepíčka, P.; Trostová, S.; Slepíčková Kasálková, N.; Kolská, Z.; Sajdl, P.; Švorčík, V. Surface Modification of Biopolymers by Argon Plasma and Thermal Treatment: Surface Modification of Biopolymers. *Plasma Process. Polym.* **2012**, *9*, 197–206. [[CrossRef](#)]
29. Juřík, P.; Slepíčka, P.; Mistrík, J.; Janíček, P.; Rimpelová, S.; Kolská, Z.; Švorčík, V. Oriented Gold Ripple-like Structures on Poly-L-Lactic Acid. *Appl. Surf. Sci.* **2014**, *321*, 503–510. [[CrossRef](#)]
30. Chen, C.-C.; Chueh, J.-Y.; Tseng, H.; Huang, H.-M.; Lee, S.-Y. Preparation and Characterization of Biodegradable PLA Polymeric Blends. *Biomaterials* **2003**, *24*, 1167–1173. [[CrossRef](#)]
31. Laput, O.; Vasenina, I.; Salvadori, M.C.; Savkin, K.; Zuza, D.; Kurzina, I. Low-Temperature Plasma Treatment of Polylactic Acid and PLA/HA Composite Material. *J. Mater. Sci.* **2019**, *54*, 11726–11738. [[CrossRef](#)]
32. Kustova, G.N.; Chesalov, Y.A.; Plyasova, L.M.; Molina, I.Y.; Nizovskii, A.I. Vibrational Spectra of WO₃·nH₂O and WO₃ Polymorphs. *Vib. Spectrosc.* **2011**, *55*, 235–240. [[CrossRef](#)]
33. Zhang, L.; Wang, H.; Liu, J.; Zhang, Q.; Yan, H. Nonstoichiometric Tungsten Oxide: Structure, Synthesis, and Applications. *J. Mater. Sci. Mater. Electron.* **2020**, *31*, 861–873. [[CrossRef](#)]
34. Al-Ajlony, A.-M.B.; Kanjilal, A.; Harilal, S.S.; Hassanein, A. Carbon Contamination and Oxidation of Au Surfaces under Extreme Ultraviolet Radiation: An x-Ray Photoelectron Spectroscopy Study. *J. Vac. Sci. Technol. B* **2012**, *30*, 041603. [[CrossRef](#)]
35. Powell, C. *X-ray Photoelectron Spectroscopy Database XPS*; NIST Standard Reference Database 20, Version 4.1.
36. Duncan, S.E.; Chang, H.-H. Implications of Light Energy on Food Quality and Packaging Selection. In *Advances in Food and Nutrition Research*; Elsevier: Amsterdam, The Netherlands, 2012; Volume 67, pp. 25–73, ISBN 978-0-12-394598-3.
37. Beu, T.A.; Mercea, P.-V. Gas Transport through Metallized Polymer Membranes. *Mater. Chem. Phys.* **1990**, *26*, 309–322. [[CrossRef](#)]
38. Prins, W.; Hermans, J.J. Theory of Permeation through Metal Coated Polymer Films. *J. Phys. Chem.* **1959**, *63*, 716–720. [[CrossRef](#)]
39. Zhang, T.; Yu, Q.; Fang, L.; Wang, J.; Wu, T.; Song, P. All-Organic Multilayer Coatings for Advanced Poly(lactic acid) Films with High Oxygen Barrier and Excellent Antifogging Properties. *ACS Appl. Polym. Mater.* **2019**, *1*, 3470–3476. [[CrossRef](#)]
40. Valerini, D.; Tammaro, L.; Vigliotta, G.; Picariello, E.; Banfi, F.; Cavaliere, E.; Ciambriello, L.; Gavioli, L. Ag Functionalization of Al-Doped ZnO Nanostructured Coatings on PLA Substrate for Antibacterial Applications. *Coatings* **2020**, *10*, 1238. [[CrossRef](#)]